Defence Technology 15 (2019) 629–635

Contents lists available at ScienceDirect

Defence Technology

journal homepage: www.elsevier.com/locate/dt

The catalytic activity of transition metal oxide nanoparticles on thermal decomposition of ammonium perchlorate

Jalpa A. Vara [a], Pragnesh N. Dave [a, b, *], Shalini Chaturvedi [c]

[a] Department of Chemistry, K S K V Kachchh University, Mundra Road, Bhuj, 370 001, Gujarat, India
[b] Department of Chemistry, Sardar Patel University, Vallabh Vidyangar, 388 120, Gujarat, India
[c] Samarpan Science and Commerce College Gandhinagar, Gujarat, India

ARTICLE INFO

Article history:
Received 11 December 2018
Received in revised form
2 February 2019
Accepted 1 April 2019
Available online 4 April 2019

Keywords:
Metal oxide nanoparticles (MONs)
Ammonium perchlorate (AP)
Catalytic activity
Activation energy

ABSTRACT

The catalytic proficiency of three MONs for AP thermal decomposition was studied in this work. A chemical co-precipitation method was used for synthesis of MONs (CuZnO, CoZnO, and NiZnO) and their characterization carried out by utilizing XRD, FTIR, and SEM. The TGA/DSC technique was employed for the investigation of the catalytic proficiency of MONs on the AP. The DSC data were used for measuring activation energy of catalyzed AP by using Ozawa, Kissinger, and Starink method. The MONs were much sensitive for AP decomposition, and the performance of AP decomposition was further improved. Among all the MONs, the CuZnO exhibits higher catalytic action than others and decomposition temperature of AP is descending around 117 °C by CuZnO. The reduction in the activation energy was noticed after the incorporation of MONs in AP.

1. Introduction

The transition metals have important utilization account in vast fields caused by its exceptional characteristics like optical, magnetic, electronic and also the catalytic proficiency [1–3]. The catalytic proficiency enhances sharply by nanometer size oxide particles than micrometer size oxide particles [4]. Nano-size materials gained attention in extreme research activities, mainly because of size effect, the optical and electronic properties and the role played by surface phenomena. The catalytic applications of transition metal oxides in the composite solid propellants [5,6]. The MONs with AP affect on the process of decomposition and the gas-phase reaction of the AP reported in literature [7]. Among propellants AP is the most vital and main oxidizing agents, it has a deciding and competitive part in the burning process [4,8–11].

AP is a stable chemical composite that gradually decompose at a low temperature. Therefore, it is important to get better or improved decomposition performance of AP to demand to generate high energy at low temperature. For that reason, the researchers are taking more interest in the thermal behavior and ignition of AP, because of its thermal behavior, AP is especially sensitive to the diminutive quantity existence of additives [4,12,13]. The investigators have described that metal oxides, such as MnO_2 [14], NiO [15], ZnO [16], CuO [17], Cu_2O [18], Co_3O_4 [19], $CuFe_2O_4$ and $MnFe_2O_4$ [9] exhibit better catalytic proficiency in the AP thermal decomposition. These minute amount additives are working like a ballistic catalyst to tailor the propellants ballistic properties. Nano-sized particles have great catalytic actions due to the small size and vast surface areas. Therefore, researchers more interested in doing better combustion performance of composite solid propellants with these nanomaterials [20–22].

In the present studies, three types of MONs (CuZnO, CoZnO, and NiZnO) have synthesized through co-precipitation route. The comparison study of three MONs as catalyst was simultaneouly studied on the AP decomposition. The catalytic ability of MONs have been measured on thermal behavior of AP by TG-DSC techniques. The Starink, KAS and FWO techniques have been applied to calculate activation energies of catalyzed AP.

2. Experimental

2.1. Reagents and chemicals

All metal nitrate and NaOH were acquired from Merck. AP was acquired from National Chemicals and used with no additional purification.

* Corresponding author. Department of Chemistry, K S K V Kachchh University, Mundra Road, Bhuj, 370 001, Gujarat, India.
E-mail address: pragneshdave@gmail.com (P.N. Dave).
Peer review under responsibility of China Ordnance Society

https://doi.org/10.1016/j.dt.2019.04.002

2.2. Synthesis of nanoparticles

The synthesis of MONs (CuZnO, CoZnO, and NiZnO) were earlier reported through co-precipitation procedure [23]. 0.2 M solution of metal nitrate (Cu, Co, and Ni) and 0.4 M zinc nitrate solution prepared. Afterward, mixing both solutions and then dropwise adding of 0.5 N NaOH with continued stirring. Keep constant pH 11–12 of the reaction till metal hydroxides precipitates. Wash the precipitates with water to make them free from nitrate ions. The brown precipitation was dried at 60 °C in the oven for 5 h and then calcined at 300 °C for 5 h.

2.3. Characterization

The characterization of all nanoparticles was done by utilizing X-ray Diffraction (powder XRD, Rigaku mini flex 600), with CuKα radiation (λ = 1.5418) and FTIR spectra were investigated by utilizing MB 3000 FTIR spectrometer (ABB Pvt. Ltd., Germany) with ATR (horizontal attenuated total reflection). The morphology of nanoparticles is characterized by utilizing Scanning Electronic Microscopy (SEM, JEOL JSM-6510 LV) with 30 kV voltages. The crystallite size was estimated by Scherrer's equation [24].

2.4. Thermal analysis

The catalytic competency of MONs investigated after the addition of MONs in AP by utilizing TG-DSC (PerkinElmer STA-8000 instrument). The virgin AP is carried out in the TG-DSC for the comparative study. All samples were recorded ~10 mg of pure AP and AP with nano-catalyst in the proportion of 99:1 in N_2 atmosphere (20 ml min^{-1}) at 10 °C·min^{-1} heating rate by using platinum crucible.

2.5. Kinetic studies

The DSC experiments carried out with three heating rate 5, 10 and 15 °C·min^{-1}. The activation energy was calculated by three methods including Flynn wall Ozawa (FWO), Starink methods and Kissinger Akahira Sunose (KAS) [25–27]. By using FWO, KAS and Starink techniques, activation energy was calculated based on Eqs. (1)–(3), respectively. The activation energy was estimated from the slope of a graph of $\ln\beta$ for FWO, $\ln(\beta/T^2)$ for KAS and $\ln(\beta/T^{1.92})$ for Starink against $1000/T$ by different (three) heating rates (β), where T_m is the peak temperature of the DSC thermogram.

$$\ln(\beta) = \ln\left(\frac{AE_a}{R}\right) - 5.331 - 1.0516\frac{E_a}{RT_m} \quad (1)$$

$$\ln\left(\frac{\beta}{T_m^2}\right) = \ln\left(\frac{AR}{E_a}\right) - \frac{E_a}{RT_m} \quad (2)$$

$$\ln\left(\frac{\beta}{T_m^{1.92}}\right) = \ln\left(\frac{AR^{0.92}}{E_a^{0.92}}\right) - 0.312 - 1.0008\frac{E_a}{RT_m} \quad (3)$$

The slope value of the plot gives the activation energy (E_a). The value of the exponential factor (A) can be estimated from the intercept of the respective plots.

3. Results and discussion

3.1. Characterization of nanoparticles

The XRD graphs of three metal incorporated ZnO nanoparticles are unleashed in Fig. 1. XRD of MONs shows sharp and high diffracted intensity of peaks, it indicates that all the particles display fine crystalline nature. The XRD diffractogram for three metal doped samples are in concurrence with the JCPDS file no 36–1451 [28]. It was simply indexed to hexagonal wurtzite phase with P63mc group. Incorporation of the metals in ZnO influences the lattice parameter of peaks and it diffuses to the crystal site, Cu, Co, and Ni are changed zinc site in the ZnO so they are enhanced the size of crystallite [29,30]. In the case of CoZnO and NiZnO two additional peaks due to secondary phase formation have been observed in the XRD spectra. Nevertheless, the extra peaks at 59.01° and 64.90° in CoZnO nanoparticles are analyzed to Co_3O_4 (JCPDS file No. 42–1467) secondary phase. Whereas, NiZnO nanoparticles confirmed the presence of two extra peaks at 74.96° and 79.07° which are analyzed to be NiO (JCPDS Card 47–1049). These may be attributed due to accomplishment of the saturated state of doping level by Cu, Co and Ni - doped ZnO nanoparticles respectively [31,32].

Broad nature of diffraction peaks due to the microstrain also indicates the nanosized nature of the prepared MONs. The crystallite size D has been obtained from the highest diffraction peak along the plane by using the Scherrer formula [24] as follows:

$$D = \frac{0.9\lambda}{\beta\cos\theta} \quad (4)$$

where λ is the wavelength of the employed CuKα radiation (0.15418 nm), β is the full width at half-maximum (FWHM) of the peaks, and θ is the Bragg angle obtained from 2θ value corresponding to maximum intensity peak in XRD pattern. The strain can be calculated by the formula:

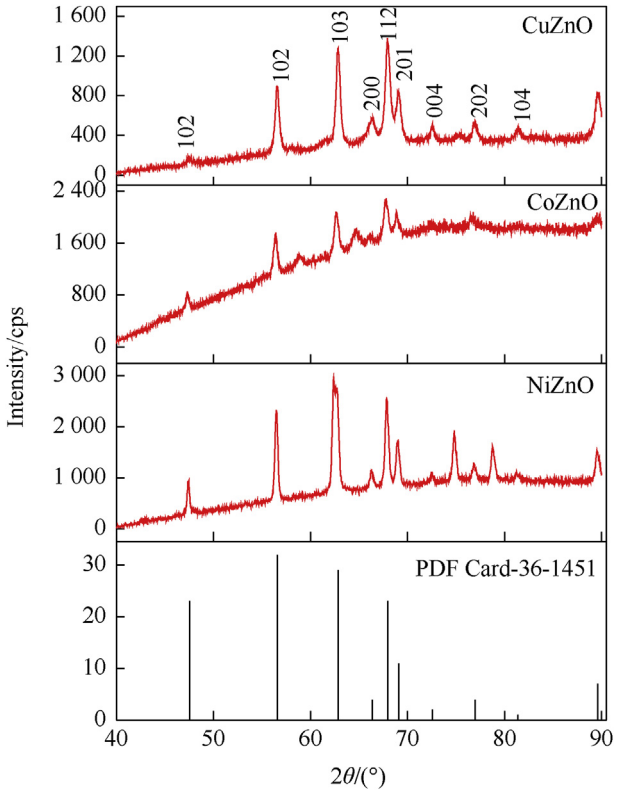

Fig. 1. XRD Pattern of metal oxide nanoparticles.

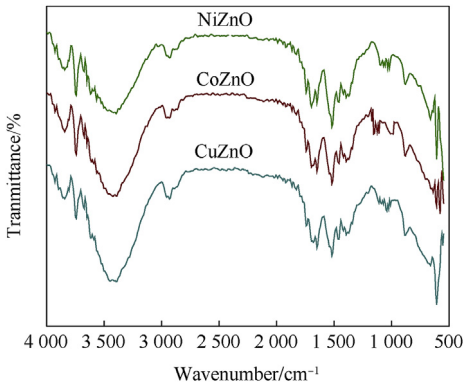

Fig. 2. FTIR graphof Metal oxide nanoparticles.

$$\varepsilon = \frac{\beta}{4\tan\theta} \tag{5}$$

The crystallite size and microstrain of the synthesized MONs is reported in Supplementary Material Table 1. The microstrain follows the order: CoZnO > CuZnO > NiZnO.

The comparative FTIR graph of CuZnO, CoZnO, and NiZnO are shown in Fig. 2, which gives complementary nature of metal oxides [33]. All the samples show broad band around ~3400 cm^{-1} in spectra which represents the O–H stretch of hydroxyl group attached on surface of metal oxide. It indicates that adsorbed H_2O molecules on metal surface during synthesis process [34,35]. The less intensive frequency band noticed at ~1640 cm^{-1} explains bending vibration (H–O–H) of hydrated water [36]. In all spectra, the intensive peaks of M – O bond of stretching vibration mode below 1000 cm^{-1} frequency region noticed, which confirms the forming of metal oxide [37,38]. The summary of all peaks are described in Supplementary Material Table 2.

The SEM images of CuZnO, CoZnO, and NiZnO nanoparticles are shown in Fig. 3. These images indicate that the shape and morphology of MONs. The images show that oxides are agglomerated. CuZnO was observed spherical in shape, and other two nanoparticles polygonal shape was observed. The image for MONs (Fig. 3) manifests the synthesized nanoparticles with reasonably uniform size distribution with some unspecified reason larger than that of the grain size obtained from XRD analysis as depicted in Table 1. This could be indicant for the formation of secondary particles by aggregation of the primary particles. For the Cu,Co and Ni doped ZnO samples, the particles seem to be more and more agglomerated, and consequently it is hard to say with greater degree about the grain size obtained from the less-resolved SEM images (Fig. 3) [39].

Table 1
Thermal analysis data of AP and AP with MONs (heating rate 10 °C min^{-1}).

Samples	DTG Peak /°C	DTA Peak /°C	DSC Peak /°C
AP	307	309	310
	390	394	395
AP + CuZnO	276	277	278
AP + CoZnO	288	288	290
AP + NiZnO	304	305	306

3.2. Catalytic activity of MONs

The thermal performance of AP in the presence of 1% MONs was investigated with 10 °C·min^{-1} heating rates by utilizing PerkinElmer STA 8000 instrument. The weight loss in the TG thermograms presented in Fig. 4 which has been coordinated with the derivative thermogravimetry (DTG) data revealed in Fig. 5. Fig. 4 offers the two-step weight loss of virgin AP at 285-425 °C temperature range [40–42]. In the initial step, 16% weight loss of pure AP occurred within the temperature range 285–350 °C coincides with the conversation of AP into intermediate products such as NH_3 and $HClO_4$. In another step, 80% of weight loss noticed to complete decomposition of AP with the formation of volatile products at higher temperature in range 350–425 °C. While adding MONs in AP, the temperature of decomposition shifted at 285-330 °C. Fig. 4 clearly depicts that the MONs has a catalytic competency over the AP decomposition. Fig. 4 is thermogram of AP with three MONs (CuZnO, CoZnO, and NiZnO) demonstrated weight loss of 98.96%, 98.55%, and 98.19% in one-step respectively. The catalytic competency of MONs on the quick oxidation of the AP gives the first step decomposition at a lower temperature.

Fig. 6 displays the DSC graph of virgin AP with three distinct peaks. The one endothermic peak is recognized at 243.12 °C that expressed the crystal structural transition from orthorhombic to cubic [43] and another two exothermic peaks demonstrated at 310.30 °C and 395.12 °C respectively. The peak noticed at 310.30 °C denotes the fractional decomposition of AP at lower temperature and another peak appeared at 395.12 °C denotes the complete decay of AP at high temperature. The incorporation of MONs with AP leads to change in the thermal decay pattern of the AP as revealed in Fig. 6. The DSC graph of MONs with AP have no variation in the endothermic peak but the exothermic peak appeared with one intense peak at 278, 290, and 306 °C for three different MONs at lower temperature and reported in Table 2. The DTA data also support to DSC data shown in Fig. 7. After incorporation of MONs with AP that lower the decomposition temperature around 90-120 °C as compared to pure AP. The rapid decomposition of AP occurred at lower temperature in the presence of MONs. CuZnO that exhibits good thermal catalytic competency on AP decomposition, which reduced the decomposition temperature around

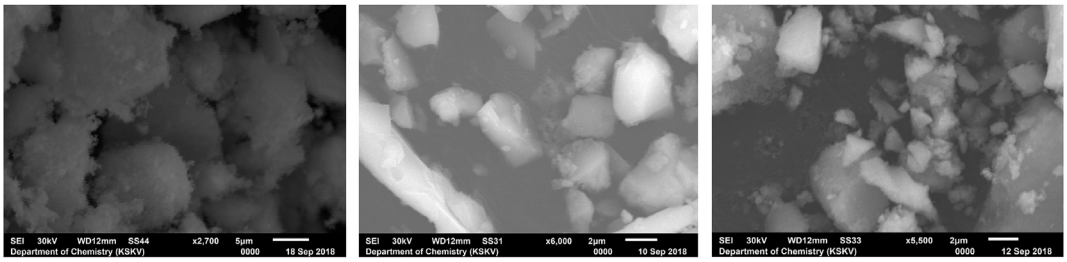

(a) CuZnO (b) CoZnO (c) NiZnO of MONs

Fig. 3. SEM images.

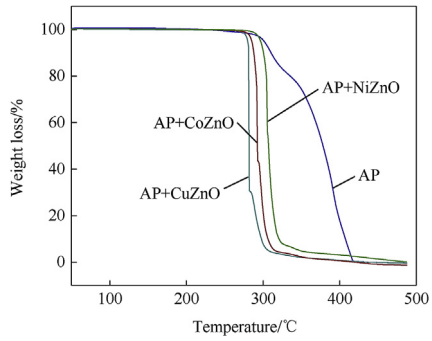

Fig. 4. TG thermogram of AP and AP with MONs (heating rate 10 °C·min^{-1}).

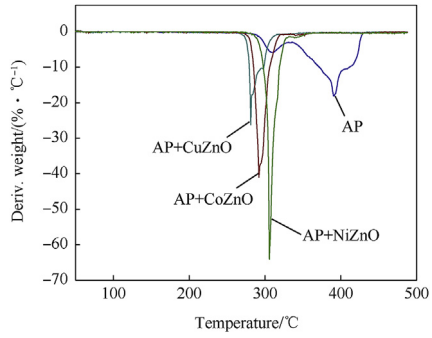

Fig. 5. DTG thermogram of AP and AP with MONs (heating rate 10 °C·min^{-1}).

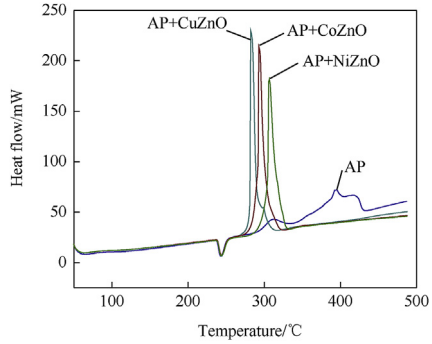

Fig. 6. DSC thermogram of AP and AP with MONs (heating rate 10 °C·min^{-1}).

117 °C.

DTA curve of virgin AP observes three main events and presented in Fig. 7. The endothermic peak is appeared at 244 °C for AP and two exothermic peaks around 309 and 394 °C. AP with MONs has obvious variation in the exothermic peak listed in Table 1 that also concord DSC results. Furthermore, our results also demonstrate that the effect of CuZnO, CoZnO and NiZnO

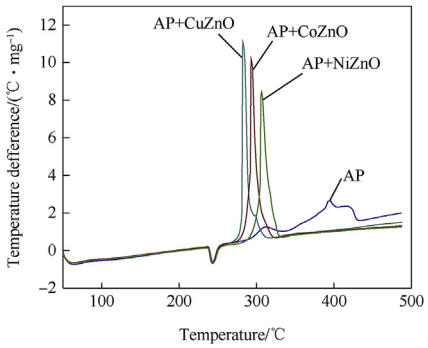

Fig. 7. DTA thermogram of AP and AP with MONs (heating rate 10 °C·min^{-1}).

nanoparticles on thermal decomposition of AP leads high temperature decomposition (HTD) shifts to low temperature decomposition (LTD). Also, it can be concluded that AP with CuZnO, CoZnO, and NiZnO nanoparticles have better catalytic proficiency on the reduction of temperature and enhancement in releasing heat than single MONs in the order of CuZnO > CoZnO > NiZnO illuminating the advantage of using MONs as catalyst in reaction process.

According to data of thermal analysis, these MONs catalysts have competency to reduce decomposition temperature of AP, presented in Table 1, CuZnO was found more proficient catalyst than the others and the decomposition temperature of AP sliding to 117 °C.

3.3. Kinetic studies

The kinetic studies of catalytic proficiency of MONs onto AP have been scrutinized by three different methods viz FWO, KAS, and Starink methods with different heating rate (5, 10, and 15 °C·min^{-1}) [25–27]. The plots of lnβ, ln(β/T^{-2}) and ln($\beta/T^{-1.92}$) against 1000/T of all samples - virgin AP and AP with MONs are presented in Fig. 8. From Table 2, the calculated values of activation energies of virgin AP are 277.58, 276.23, and 276.47 kJ mol^{-1} by FWO, KAS, and Starink respectively. After addition of MONs, activation energy reduces significantly. The results point out that CuZnO has excellent catalytic proficiency in order to increase AP decomposition rate. Table 2 displays the lower in activation energy for AP in compare to MONs. The correlation coefficient (r) is close to one. The activation energy decreases with decreasing the exponential factor inturn the catalytic proficiency increases.

In the DSC based thermokinetics, activation energy of KAS and Starink techniques are similar to each other and lesser than the FWO method. The equations used in the KAS and Starink techniques have almost same activation energy that is pointed out from the results. These parameters are achieved from the dependence of exothermic peak temperatures established in a role of heating velocity. The Kissinger correlation can be used to define the relationship concerning the decomposition temperature and heating rate [44]. The MONs have broad surface area caused by their very

Table 2
Thermokinetics data of AP, AP with MONs by using Ozawa, Kissinger and Starink methods.

Sample	FWO			KAS			Starink		
	Ea/kJ·mol^{-1}	ln A/min^{-1}	R^2	Ea/kJ·mol^{-1}	ln A/min^{-1}	R^2	Ea/kJ·mol^{-1}	ln A/min^{-1}	R^2
AP	277.48	4.05	0.995	276.23	16.00	0.995	276.46	12.49	0.995
AP + CuZnO	164.97	3.94	0.960	164.32	9.99	0.955	164.56	8.19	0.955
AP + CoZnO	180.20	3.97	0.995	180.18	10.86	0.995	180.11	8.83	0.995
AP + NiZnO	168.99	3.93	0.998	168.13	10.17	0.998	168.38	8.31	0.998

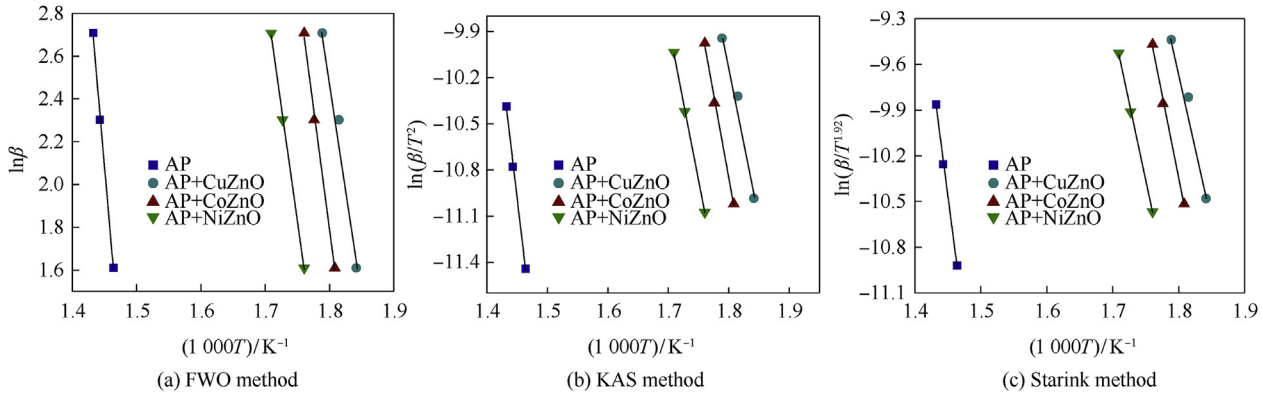

Fig. 8. Plot of AP and APwith threeMONs by using FWO, KAS and Starink methods.

small size and there are many reactive sites over the surface. The promotions of reactions endorsed by MONs with involvement absorbing the gaseous reactive molecules on their surface in the exothermic decomposition.

The results stated that the decomposition of AP from intermediate products to gaseous products in presence of CuZnO nanoparticle has a superior catalytic activity in comparison to CoZnO, and NiZnO. The activation energy of decomposition AP with CuZnO nanoparticles reduced, exhibiting distinguishable kinetic parameters of a self-increasing reaction.

3.4. Mechanism of thermal decomposition of AP

The thermal decomposition of AP studies by two most significant mechanisms. The first electron shift from perchlorate ion to ammonium ion and second proton shift from ammonium ion to perchlorate ion, but proton transfer is more acceptable as follows [7,45–50]:

$$NH_4ClO_{4(s)} \rightarrow NH_4^+ + ClO_4^- \rightarrow NH_{3(s)} + HClO_{4(s)} \rightarrow NH_{3(g)} + HClO_{4(g)}$$

The AP decomposition gives two most important products NH_3 and $HClO_4$ identified in the experiments by the researcher [7,47–49]. This postulates that the primary point of AP decomposition process is proton shift. This mechanism includes three important steps: The step-1, includes a pair of ions in AP lattice. The step-2, includes decay or sublimation step that begins with proton movement starting from the cation NH_4^+ to the anion ClO_4^-, then the molecular complex is formed and decomposes into NH_3 and $HClO_4$ in step-3. The molecules of NH_3 and $HClO_4$ also react in the adsorbed layer on the surface of perchlorate or desorbs and inspiring relating in the gas phase [45]:

$$NH_4ClO_4 \leftrightarrow NH_3 - H - ClO_4 \leftrightarrow NH_3 - HClO_4 \leftrightarrow NH_{3(a)} + HClO_{4(a)} \leftrightarrow NH_{3(g)} + HClO_{4(g)}$$

The absorption of gaseous reactive molecules on the surface MONs which enhances reaction rate by the proton transfer mechanism. The increment observed in the thermal decay rate of AP is by virtue of increasing the development of more holes within the *p*-type semiconducting area. The mechanism of catalytic efficiency of catalyst is in the interest of the O_2^- ion on the exterior part of the catalyst. The O_2^- formed throughout decomposition of AP and the surface O_2^- of catalysts are likely the proton traps through the following reaction [50,51]:

$$2NH_4^+ + O^{2-} \rightarrow H_2O + 2NH_3$$

The involvement of catalyst in O_2^- formation and gas absorption on its surface are main reasons in the completion of AP thermal decay. The CuZnO nanoparticles surface is able to produce more O_2^- in comparison with other CoZnO and NiZnO NPs. Therefore, CuZnO nanoparticles are increasing in quick progression of AP thermal decay than others.

The perfect mechanism of thermal decay of AP has not understood totally yet. The mechanism of AP thermal decay through chain reaction has been proposed by YU Zongxue's [52]. The NH_3, H_2O and a minor quantity of N_2O and O_2 are forming during the low-temperature thermal decay of AP. The HCl, H_2O, N_2O, NH_3, Cl_2, NO, O_2, NO_2 and a minor quantity of ClO_2 have been formed in the high-temperature point of AP decay.

At low temperature:

$$NH_4ClO_4 \rightarrow NH_4^+ + ClO_4$$

$$NH_4^+ + ClO_4 \rightarrow NH_3 + HClO_4$$

$$4HClO_4 \rightarrow 2ClO_3 + 2ClO + 3O_2 + 2H_2O$$

$$2NH_3 + 2O_2 \rightarrow N_2O + 3H_2O \leftrightarrow NH_4NO_3 + H_2O$$

At high temperature:

$$4HClO_4 \rightarrow Cl_2 + 5O_2 + 2ClO_2 + H_2O$$

$$2Cl_2 + 2H_2O \rightarrow 4HCl + O_2$$

$$2NH_3 + 2ClO_2 \rightarrow N_2O + Cl_2 + 3H_2O$$

$$N_2O + O_2 \rightarrow NO + NO_2$$

The mechanism of AP combustion has been investigated by many research workers and role of condensed phase reaction at a pressure around 10–14 MPa is critical in many types of studies. The decomposition of AP occurs more than 70% in the condensed phase [53–55].

4. Conclusion

The three different types of $CuZnO_2$, $CoZnO_2$, and $NiZnO_2$ nanoparticles were synthesized via co-precipitation procedure. The study presents a new way to get better thermal decomposition of

AP through synthesized MONs. Thermal analysis techniques including TGA-DSC, DTA and DTG were applied to study thermal responses. The CuZnO showed superior catalytic action than $CoZnO_2$, and $NiZnO_2$ and shifting decomposition temperature at 117 °C in downhill for AP.

The thermal decomposition temperature was found in the order CuZnO > CoZnO > NiZnO nanoparticles and all three MONs have good catalytic activity. The results prove that activation energies of AP with MONs are lower than virgin AP. So, AP with MONs can be promising candidates for solid propellants for energetic materials.

Acknowledgement

The authors are grateful to the Department of Chemistry, KSKV Kachch University, Bhuj for laboratory facility and for XRD, SEM and TGA-DSC analysis and also thankful to Chemistry Department, Sardar Patel University, Vallabh Vidyanagar for providing ATR-FTIR instrument facility.

Appendix A. Supplementary data

Supplementary data to this article can be found online at https://doi.org/10.1016/j.dt.2019.04.002.

References

[1] Hinklin TR, Azurdia J, Kim M, Marchal JC, Kumar S, Laine RM. Finding spinel in all the wrong places. Adv Mater 2008;20:1373–5.
[2] Yoon TJ, Kim JS, Kim BG, Yu KN, Cho MH, Lee JK. Multifunctional nanoparticles possessing a Magnetic Motor Effect for drug or gene delivery. Angew Chem Int Ed 2005;44:1068–71.
[3] Marco JF, Gancedo JR, Gracia M, Gautier JL, Rios EI, Palmer HM, Greaves C, Berry FJ. Cation distribution and magnetic structure of the ferrimagnetic spinel $NiCo_2O_4$. J Mater Chem 2001;11:3087–93.
[4] Boldyrev VV. Thermal decomposition of ammonium perchlorate. J Thermochim Acta 2006;443:1–36.
[5] Reid DL, Russo AE, Carro RV, Stephens MA, Lepage AR, Spalding TC, Petersen EL, Seal S. Nanoscale additives tailor energetic materials. Nano Lett 2007;7:2157–61.
[6] Chaturvedi S, Dave PN. Nano-metal oxide: potential catalyst on thermal decomposition of ammonium perchlorate. J Exp Nanosci 2012;7:205–31.
[7] Joshi SS, Patil PR, Krishnamurthy VN. Thermal decomposition of ammonium perchlorate in the present of nanosized ferric oxide. Def Sci J 2008;58:721–7.
[8] Singh G, Kapoor IPS, Dubey S, Siril PF. Preparation, characterization and catalytic activity of transition metal oxide nanocrystals. J Sci Conf Proc 2008;1:7–14.
[9] Singh G, Kapoor IPS, Dubey S, Siril PF. Kinetics of thermal decomposition of ammonium perchlorate with nanocrystals of binary transition metal perrites. Propellants, Explos Pyrotech 2009;34(1):72–7.
[10] Zhu J, Li D, Chen H, Yang X, Lu L, Wang X. Highly dispersed CuO nanoparticles prepared by a novel quick-precipitation method. Mater Lett 2004;58:3324–7.
[11] Liu L, Li F, Tan L, Miang L, Yi Y. Effects of nanometer Ni, Cu, Al and NiCu powders on the thermal decomposition of ammonium perchlorate. Propellants, Explos Pyrotech 2004;29(1):34–8.
[12] Jacob PWM, Whitehead HM. Decomposition and combustion of ammonium perchlorate. Chem Rev 1969;69:551–90.
[13] Keenan AG, Siegmund RF. Thermal decomposition of ammonium perchlorate. Q Rev Chem Soc 1969;23:430–52.
[14] Chena Y, Mab K, Wanga J, Gaoa Y, Zhua X, Zhanga W. Catalytic activities of two different morphological nano-MnO_2 on the thermal decomposition of ammonium perchlorate. Mater Res Bull 2018;101:56–60.
[15] Li Z, Xiang X, Bai L, Li F. A nanocomposite precursor strategy to mixed-metal oxides with excellent catalytic activity for thermal decomposition of ammonium perchlorate. Appl Clay Sci 2012;65–66:14–20.
[16] Sun X, Qiu X, Li L, Li G. ZnO twin-cones: synthesis, photoluminescence, and catalytic decomposition of ammonium perchlorate. Inorg Chem 2008;47(10):4146–52.
[17] Gheshlaghi EA, Shaabani B, Khodayari A, Kalandaragh YA, Rahimi R. Investigation of the catalytic activity of nano-sized CuO, $Co_3O_4$and $CuCo_2O_4$ powders on thermal decomposition of ammonium perchlorate. Powder Technol 2012;217:330–9.
[18] Heng B, Xiao T, Hua X, Yuan M, Tao W, Huang W, TangY. Catalytic activity of Cu_2O micro-particles with different morphologies in the thermal decomposition of ammonium perchlorate. Thermochim Acta 2011;524(1–2):135–9.
[19] Xu C, Wang X, Zhu J, Yang X, Lu L. Deposition of Co_3O_4nanoparticles onto exfoliated graphite oxide sheets. J Mater Chem 2008;18:5625–9.
[20] Ishitha K, Ramakrishna PA. Studies on the role of iron oxide and copper chromite in solid propellant combustion. Combust Flame 2014;10:2717–28.
[21] Babuk VA, Dolotkazin I, Gamsov A, Glebov A, DeLuca LT, Galfetti L. Nano-aluminum as a solid propellant fuel. J Propuls Powder 2009;25:482–9.
[22] DeLuca LT, Galfetti L. Burning of metallized composite Solid rocket propellants: from micrometric to nanometric aluminum size, 4th Asian Joint Conference on Propulsion and Power. Korea: Gyeongju; 2008.
[23] Singh G, Kapoor IPS, Dubey S, Siril PF, Hua YJ, Zhao FQ, Hu RZ. Effect of mixed ternary transition metal ferrite nanocrystallites on thermal decomposition of ammonium perchlorate. Thermochem Acta 2008;477:42.
[24] Birks LS, Friedman H. Particle size determination from X-Ray line broadening. J Appl Phys 1946;17(8):687.
[25] Cheng Y, Li Y, Yan S, Huang C. Deviation of activation energy caused by neglecting a temperature term in Ozawa Equation. J Math Chem 2010;48:704.
[26] Chen T, Du P, Jiang W, Liu J, Hao G, Gao H, Xiao L, Ke X, Zhao F, Xuan C. A facile one-pot solvothermal synthesis of $CoFe_2O_4$/RGO and its excellent catalytic activity on thermal decomposition of ammonium perchlorate. RSC Adv 2016;6:83838.
[27] Starink MJ. The determination of activation energy from linear heating rate experiments: a comparison of the accuracy of isoconversion methods. Thermochim Acta 2003;404:163.
[28] Ghomi JS, Ghasemzadeh MA, Zahedi S. ZnO nanoparticles a highly effective and readily recylable catalyst for the one pot synthesis of 1, 8-dioxo-decahydroacridine and 1,8-dioxoctahydro-xanthene derivatives. J Mex Chem Soc 2013;57(1):1–7.
[29] He R, Tang B, Ton-That C, Phillips M, Tsuzuki T. Physical structure and optical properties of Co-doped ZnO nanoparticles prepared by co-precipitation. J Nanoparticle Res 2013;15(11):1–8.
[30] Chauhan J, Shrivastav N, Dugaya A, Pandey D. Synthesis and characterization of Ni and Cu doped ZnO. J Nanomed Nanotechnol 2017;8(2):1–8.
[31] Pal B, Sarkar D, Giri PK. Structural, optical, and magnetic properties of Ni doped ZnO nanoparticles: correlation of magnetic moment with defect density. Appl Surf Sci 2015;356:804–11.
[32] Liu Y, Liu H, Chen Z, Kadasala N, Mao C, Wang Y, Zhang Y, Liu H, Liu Y, Yang J, Yan Y. Effects of Ni concentration on structural, magnetic and optical properties of Ni-doped ZnO nanoparticles. J Alloy Comp 2014;604:281–5.
[33] Melendres CA, Bowmaker GA, Leger JM, Beden B. In-situ synchrotron far infrared spectroscopy of surface films on a copper electrode in aqueous solutions. J Electroanalytical Chem 1998;449:215–8.
[34] Waldron RD. Infrared spectra of ferrites. J Phys Rev 1955;99:1727–35.
[35] Luisetto I, Pepe F, Bemporad E. Preparation and characterization of nano cobalt oxide. J Nanoparticle Res 2008;10:59–67.
[36] Verelst M, Ely TO, Amiens C, Snoeck E, Lecante P, Mosset A, Respaud M, Broto JM, Chaudret B. Synthesis and characterization of CoO, Co_3O_4 and mixed Co/CoO nanoparticules. Chem Mater 1999;11:2702–8.
[37] Niasari MS, Mir N, Davar F. Synthesis and characterization of Co_3O_4nanorods by thermal decomposition of cobalt oxalate. J of Phys and Chem of Solids 2009;70:847–52.
[38] Gabal MA, El-Bellihi AA, Ata-Allah SS. Effect of calcinations temperature on Co(II) oxalate dehydrate-iron(II) oxalate dihydrate mixture: DTA–TG, XRD, Mossbauer, FT-IR and SEM studies. Mater Chem Phys 2003;81:84–92.
[39] Sajjada M, Ullaha I, Khanb MI, hanc J, Khana MY, Qureshid MT. Structural and optical properties of pure and copper doped zinc oxide nanoparticles. Results in Physics 2018;9:1301–9.
[40] Jacobs PMW, Parasone GS. Mechanism of the decomposition of ammonium perchlorate. J Combust Flame 1969;13:419–25.
[41] Rosser WA, Inami SH. Thermal decomposition of ammonium perchlorate. J Combust Flame 1968;12:427–35.
[42] Kishore K, Sridhara K. Solid propellant chemistry: condensed phase behaviour of ammonium perchlorate based solid propellants, vol 10. New Delhi: DESIDOC; 1990.
[43] Zhi J, Feng-Qi Z. Study on effects of nanometer metal powder on thermal decomposition of HMX. J Propuls Technol 2002;23:258–61.
[44] Burnhamb AK, Vyazovkin S, Criadoc JM, Perez-Maquedac LA, Popescud C, Sbirrazzuolie N. ICTAC Kinetics Committee recommendations for performing kinetic computations on thermal analysis data. Thermochim Acta 2011;520:1–19.
[45] Zhao S, Ma D. Preparation of $CoFe_2O_4$nanocrystallites by solvothermal process and its catalytic activity on the thermal decomposition of ammonium perchlorate. J Nanomater 2010;2010:1–5.
[46] Wang Y, Xia X, Zhu J, Li Y, Wang X, Hu X. Catalytic activity of nanometer-sized CuO/Fe2O3 on thermal decomposition of AP and combustion of AP-based propellant. Combust Sci Technol 2011;183:154–62.
[47] Singh G, Kapoor IPS, Dubey S, Siril PF. Preparation, characterization and catalytic activity of transition metal oxide nanocrystals. J Sci Conf Proc 2009;1:11–7.
[48] Liu T, Wang L, Yang P, Hu B. Preparation of nanometer $CuFe_2O_4$ by autocombustion and its catalytic activity on the thermal decomposition of ammonium perchlorate. Mater Lett 2008;62:4056–8.
[49] Xu H, Wang X, Zhang L. Selective preparation of nanorods and microoctahedrons of Fe_2O_3 and their catalytic performances for thermal decomposition of ammonium perchlorate. Powder Technol 2008;185:176–80.
[50] Li L, Sun X, Qiu X, Xu J, Li G. Nature of catalytic activities of CoOnanocrystals in thermal decomposition of ammonium perchlorate. Inorg Chem 2008;47:8839–46.
[51] Chen L, Li L, Li G. Synthesis of CuOnanorods and their catalytic activity in the

thermal decomposition of ammonium perchlorate. J Alloy Comp 2008;464:532–6.
[52] Yu Z, Chen L, Lu L, Yang X, Wang X. DSC/TG-MS study on in situ catalytic thermal decomposition of ammonium perchlorate over CoC_2O_4. Chin J Catal 2009;30(1):19–23.
[53] Sinditskii VP, Egorshev VY, Serushkin VV, Levshenkov AI, Berezin MV, Filatov SA, Smirnov SP. Evaluation of decomposition kinetics of energetic materials in the combustion wave. Thermochim Acta 2009;496(1):1–12.
[54] Sinditskii VP, Egorshev VY, Serushkin VV, Levshenkov AI, Berezin V M, Filatov SA. Combustion of energetic materials governed by reactions in the condensed phase. Int J Energetic Mater Chem Propuls 2010;9(2):147–92.
[55] Sinditskii VP, Egorshev VY, Serushkin VV, Levshenkov AI, Berezin MV, Filatov SA. Combustionof energetic materials controlled by condensed-phase reactions. Combust Explos Shock Waves 2012;48(1):81–99.